scientific reports

OPEN

Comparison of acid exfoliators in carbon nanosheets synthesis from stinging nettle (*Urtica dioica*) for electrochemical applications

Kanokon Nuilek[1,2][✉], Winadda Wongwiriyapan[3], Vichuda Sattayarut[3], Andrea Simon[1], Daniel Koncz-Horváth[2], Tibor Ferenczi[4], Ferenc Kristály[5] & Peter Baumli[2][✉]

Carbon nanosheets (CNs) were successfully synthesized from nettle stem (NS) which is an inexpensive material with a high carbon content that is abundantly available in nature. CNs were produced using chemical (potassium hydroxide activation and acid exfoliation) and thermal treatments. Sulfuric (H_2SO_4), phosphoric (H_3PO_4) and nitric (HNO_3) acid solutions were used for exfoliation. CNs exfoliated by H_3PO_4 have higher specific surface area (789 m^2 g^{-1}) compared to CNs exfoliated by H_2SO_4 (705 m^2 g^{-1}) and HNO_3 (106 m^2 g^{-1}). In this work, NSCNs were found to be a potential candidate for electrode material in electrochemical capacitors. The maximum specific capacitance of the NSCNs exfoliated by H_3PO_4 is found to be 27.3 F g^{-1} at a current density of 0.05 A g^{-1}, while the specific capacitance of NSCNs exfoliated by H_2SO_4 and HNO_3 is 9.34 F g^{-1} and 1.71 F g^{-1}, respectively. Energy density (0.06–0.95 Wh kg^{-1}) and power density (20.9–26.7 W kg^{-1}) of NSCNs are confirmed to be supercapacitor materials and can be applied in energy storage devices.

2D carbon nanostructures – namely graphene and carbon nanosheets – are increasingly being researched as candidates for energy storage devices such as batteries or capacitors[1–3]. Carbon nanotubes, nanofibers and nanosheets[4–7] have been well documented. Glass-like carbon is a vital type of the carbon family, typically referred to as glassy carbon or vitreous carbon. Glassy carbon, described as amorphous carbon, is non-graphitizing and contains mostly sp^2 sites. The properties of carbon are a combination of those of glass and ceramic materials, characterized by low density, high thermal and chemical resistance[8,9]. The preparation of carbon nanostructures is carried out by chemical and thermal treatments. Potassium hydroxide (KOH) activation is a well-known method to generate a pore network in carbons and to expand the carbon layers. Chemical acids are used as intercalating agents to obtain exfoliated graphite by different processes[10–13]. This activated carbon can be obtained from various agricultural wastes[14,15].

The preparation of nanostructured materials from waste materials has drawn tremendous interest in recent years[16,17]. Many researchers have demonstrated that carbon materials for use as adsorbent or electronic materials can be synthesized by potassium hydroxide from low-cost waste materials such as rice husk[18], Acai stone[19], corncob[20], pine cone flower[21], banana peel[22], water hyacinth[23], waste coffee grounds[24], pineapple leaf fibre[25], bamboo[26], wood sawdust[27], peanut shell[28–30], jute[31], gulfweed[32] and pomelo peel[33]. Nettle (*Urtica dioica*) is a plant widely distributed in many areas of Asia, Europe, America and Africa[34]. Nettle is considered as waste material mostly used for agricultural purposes or discarded as garbage. Natural structures of nettle consist of cellulose, hemicellulose and lignin[35], which can be an important precursor in the preparation of highly ordered carbons and contribute to the porosity of biochar yield[36,37]. Moreover, both nettle stems and leaves can be used to produce carbon. Hierarchical porous carbon derived from nettle leaves has been studied for used in advanced supercapacitors and lithium-ion batteries[38].

One promising area of application for activated carbon is in energy storage and delivery. Ultracapacitors, also called electric double-layer electrodes, are the new range of supercapacitors and are highly efficient in energy

[1]Institute of Ceramics and Polymer Engineering, University of Miskolc, Miskolc 3515, Hungary. [2]Institute of Metallurgy, Metal Forming and Nanotechnology, University of Miskolc, Miskolc 3515, Hungary. [3]College of Nanotechnology, King Mongkut's Institute of Technology Ladkrabang, Chalongkrung Rd., Ladkrabang, Bangkok 10520, Thailand. [4]Institute of Metallurgy, University of Miskolc, Miskolc 3515, Hungary. [5]Institute of Mineralogy and Geology, University of Miskolc, Miskolc 3515, Hungary. [✉]email: k.nuilek@gmail.com; fembaumli@uni-miskolc.hu

Sample		Chemical composition (wt.%)		
activation	Exfoliation	C	O	Other
Dried nettle stem	50.80	36.03	13.17	
KOH	-	93.84	4.78	1.38
KOH	HNO$_3$	88.52	10.51	0.97
KOH	H$_2$SO$_4$	88.71	9.38	1.91
KOH	H$_3$PO$_4$	90.96	7.70	1.34

Table 1. Chemical composition (EDS) of the dried NS, activated NS, NSCNs exfoliated by HNO$_3$, H$_2$SO$_4$ or H$_3$PO$_4$.
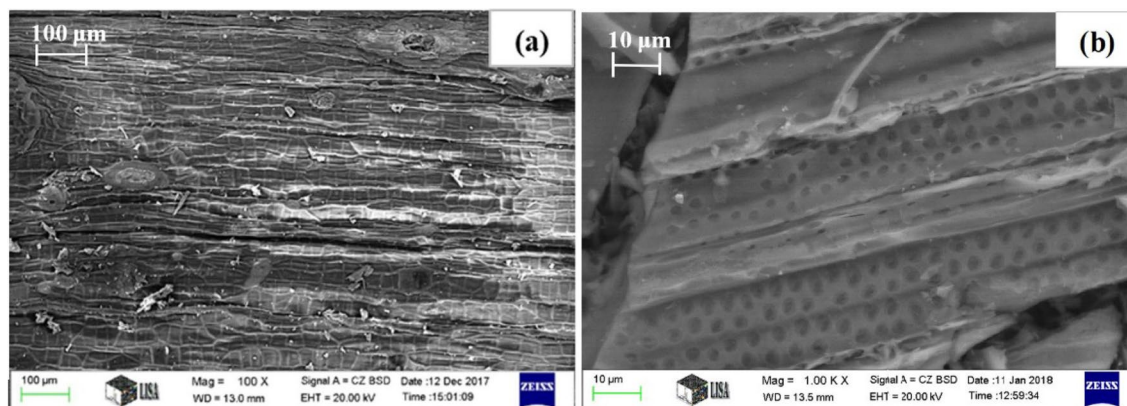
Figure 1. SEM micrographs of (**a**) dried and (**b**) KOH activated nettle stems.

storage and delivery characteristics compared to batteries. They are able to deliver high rates of energy involving a mechanism of simple charge separation at the interface between electrode and electrolyte[39,40]. As follows from Ragone plots of the power density against energy density, the efficiency of a supercapacitor depends on the electrode material. Hence, the quest for novel materials for electrodes[41] involves activated carbon materials owing to their high specific surface area and charge storage[42]. No previous studies have reported on using nettle as a raw material for producing carbon nanosheets by chemical activation and exfoliation process. The activated carbon produced in this way can be used as adsorbent or electrode materials for supercapacitors.

The goal of this work is to systematically investigate the mechanism of different acid activations during the exfoliation process and their effects on the properties of synthesized carbon nanosheets prepared from waste nettle stem. Phosphoric, sulfuric and nitric acid are used in the experiments to examine the influence of triprotic, diprotic and monoprotic acids on the synthesis of carbon nanosheets.

Results and discussion

Organic, chemical composition and microstructure of materials.
Nettle is mainly composed of cellulose, lignin and hemicellulose (49.8 wt.%, 11.9 wt.% and 15.3 wt.%, respectively). The results of the chemical composition obtained from EDS are listed in Table 1. Due to its high cellulose and carbon content, nettle stem was used to prepare carbon nanostructure, as its carbon content can be further increased by the activation and carbonization processes[17,43].

The microstructure of the dried nettle stem (Fig. 1a) reveals a groove and hollow surface, composed of a fibrous structure with many hollow stinging hairs called trichomes. The cell wall in the fibre is inhomogeneous, layered and mainly composed of cellulose, lignin and hemicellulose. After activation, a large number of angular and flake particles and micropores were found on the surface (Fig. 1b). Potassium reacts intensely with the dried nettle stem and pulls apart the layers. Activation increases the carbon content to 93.84 wt.% with a small amount of contaminants.

The exfoliation process was carried out by using one of three different acids: sulfuric, phosphoric and nitric acid. The SEM micrograph of NSCNs exfoliated by H$_2$SO$_4$ (Fig. 2a) shows a smooth surface and clearly reveals the formation of separated carbon nanosheets with thickness ranging from ~42 to 71 nm. EDS results demonstrated that carbon nanosheets mainly contain carbon (88.71 wt.%). In the structure of NSCNs exfoliated by H$_3$PO$_4$ (Fig. 2b), ultra-thin structures and overlapping carbon nanosheets were identified, with the thickness of carbon nanosheets ranging from 49 to 60 nm. Exfoliation with phosphoric acid yielded the highest carbon content (90.96 wt.%) among the exfoliated specimens. Angular, thin sheets were found in NSCNs exfoliated by HNO$_3$, with thicknesses varying from 89 to 95 nm (Fig. 2c), and 88.52 wt.% carbon.

The structure of the produced carbon nanosheets after exfoliating by three different acids are quite similar (Fig. 2a–c); the carbon nanosheets are separated and their surface is clean. The major presence of the element carbon indicates the high purity of these samples. All exfoliating agents (H$_2$SO$_4$, H$_3$PO$_4$ and HNO$_3$) were suitable
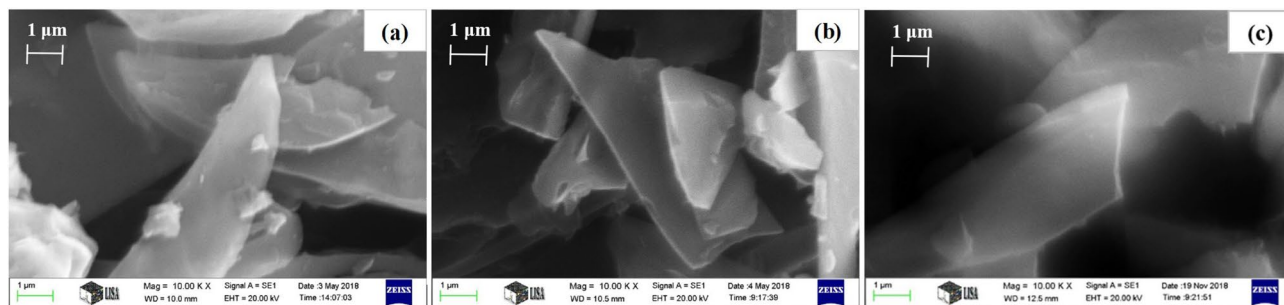
Figure 2. SEM micrographs of the NSCNs exfoliated by (**a**) H_2SO_4 (**b**) H_3PO_4 and (**c**) HNO_3.
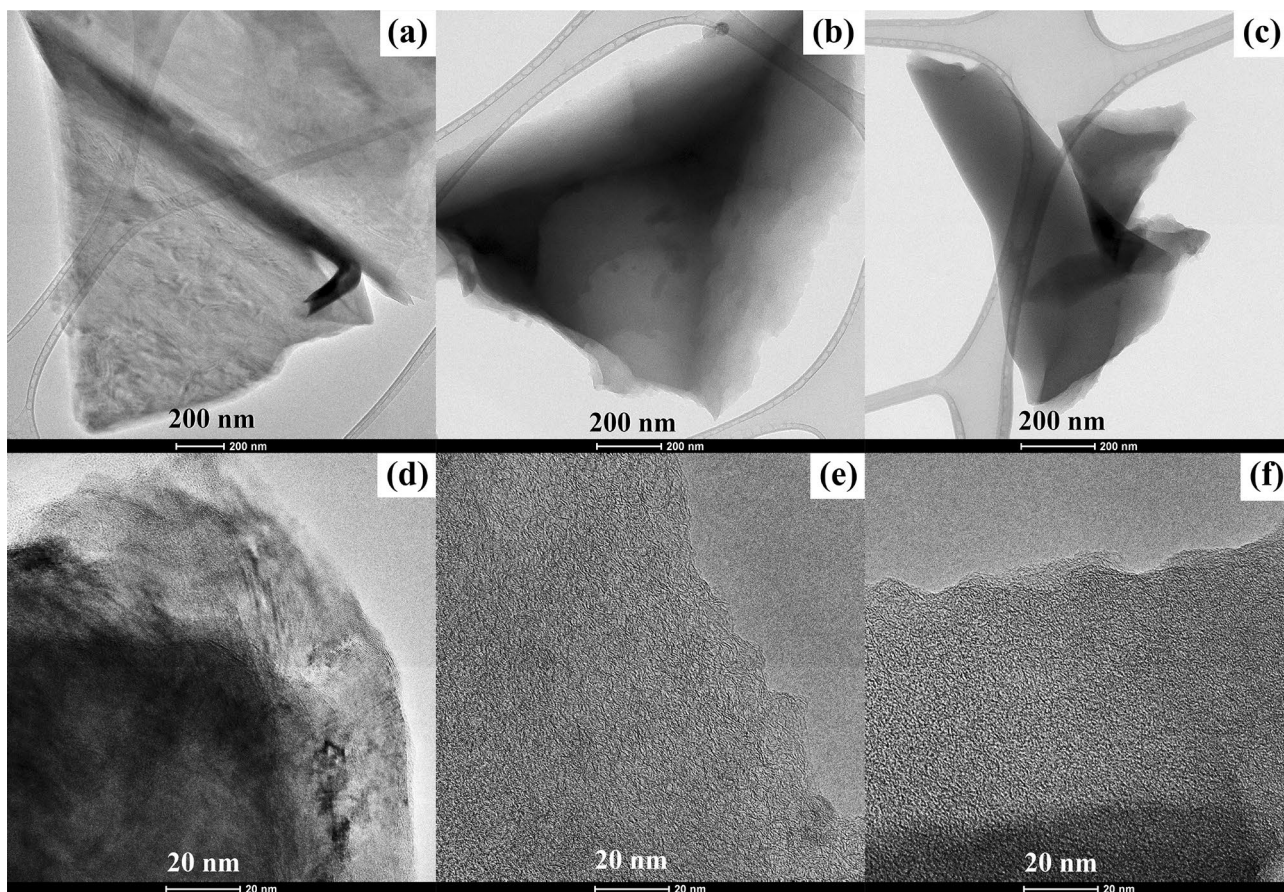
Figure 3. TEM (**a–c**) and HRTEM (**d–f**) micrographs of the NSCNs exfoliated by (**a, d**) H_2SO_4. (**b, e**) H_3PO_4 or (**c, f**) HNO_3.

to disrupt the layers in the material. During the exfoliation process, acids intercalated into the carbon layers and ruptured interlayer bonds. The exfoliation process increased the specific surface area of the carbonaceous materials (Fig. 5).

TEM images (Fig. 3a–c) reveal the amorphous two-dimensional nanosheet porous structure of NSCNs. In the TEM images, the bright and transparent regions are the ultrathin nanosheet and the less transparent areas reveal the overlapped or folding areas of NSCNs, which further imply the ultrathin structure. The structure of the exfoliated NSCNs was explored further with high resolution TEM (HRTEM) imaging (Fig. 3d–f). The layered nanosheet structure is highly porous and gradually becomes thinner toward the edges of the material. NSCNs have a monolayer property, further demonstrating their ultrathin nature[4]. The pore distribution can be seen by the white dots in the grey areas from HRTEM images[3].

Structure of carbon nanosheets. Figure 4 exhibits X-ray diffractograms of NSCNs. A glassy carbon structure[44–46] develops in the exfoliated samples. Both the large peaks at $2\theta = \sim 22°$ and $44°$ and the weak and broad diffraction peak occurring in the 2θ range $79°$–$81°$ (Table 2) can be attributed to the typical glassy amorphous carbon structure. The XRD patterns of the different samples are quite similar. This suggests that the exfo-
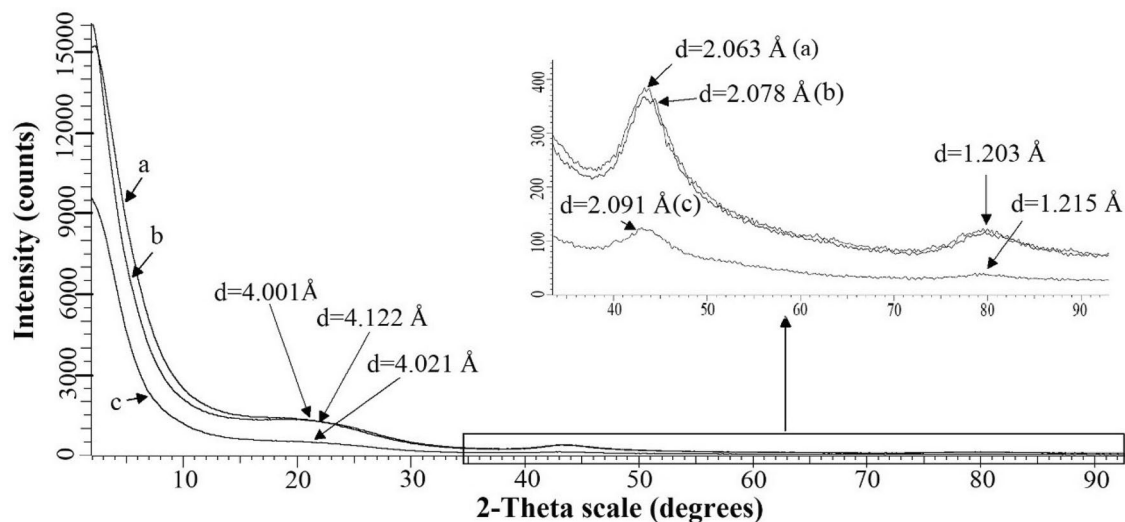
Figure 4. XRD patterns of nettle stem carbon nanosheets exfoliated by (**a**) H_2SO_4, (**b**) H_3PO_4 or (**c**) HNO_3.

	d-value (Å)		
Exfoliating acid	**1st ($2\theta = \sim 22°$)**	**2nd ($2\theta = 44°$)**	**3rd ($2\theta = \sim 80°$)**
H_2SO_4	4.001	2.063	1.203
H_3PO_4	4.122	2.078	1.203
HNO_3	4.021	2.091	1.215

Table 2. Peak positions and d values of XRD pattern of NSCNs exfoliated by different acids.

liating acid does not have a significant effect on the structure of the nettle stem carbon nanosheet. Moreover, the acid and KOH solution do not dissolve the carbon material.

Surface properties. Physical properties including the specific surface area and the micropore volume of NSCNs were measured using the Brunauer–Emmett–Teller (BET) method based on nitrogen gas adsorption and desorption, as porous materials are also defined in terms of their adsorption properties. The specific surface area and micropore volume of dried nettle stem are found to be 0.17 $m^2\ g^{-1}$ and 0.0001 $cm^3\ g^{-1}$, respectively. The specific surface area of NSCNs exfoliated by H_3PO_4, H_2SO_4 and HNO_3 are 789, 705 and 106 $m^2\ g^{-1}$, respectively. Micropore volume of NSCNs exfoliated by H_3PO_4, H_2SO_4 and HNO_3 is 0.33, 0.29 and 0.04 $cm^3\ g^{-1}$, respectively. Pore diameters in the exfoliated NSCNs were less than 3 nm. The effect of the phosphoric acid on the surface area of the carbon is stronger than that of the nitric and sulfuric acid by 10.6% and 86.5%, respectively. On the other hand, phosphoric acid has more effect on the change of carbon microporous volume than nitric and sulfuric acid by 9.4% and 87.5%, respectively.

During activation, KOH can penetrate the pores of the carbonized material. Interlayered KOH residue can react with the exfoliation acids (H_2SO_4, H_3PO_4 and HNO_3), thus some chemical compounds, such as K_2SO_4, K_3PO_4 and KNO_3, may form. The molar volume of K_3PO_4, K_2SO_4 and KNO_3 is 82.79, 65.51 and 47.94 $cm^3\ mol^{-1}$, respectively. Based on their thermochemical properties (from the database of HSC Chemistry)[47], all these compounds can form due to negative $\Delta_f G$. The $\Delta_f G$ of K_3PO_4, K_2SO_4 and KNO_3 is -1876.38, -1319.67 and -394.70 kJ mol^{-1}, respectively. These compounds cause stress in the pores of the activated carbon. As K_3PO_4 has a 26.4 or 72.7% higher molar volume than K_2SO_4 or KNO_3, respectively, it generates the highest specific surface area and micropore volume in KOH activated carbon nanosheets (Fig. 5).

Based on the results of nitrogen adsorption, pore structure can be divided into 6 classes according to the IUPAC classification[48]. The results from nitrogen adsorption isotherms (Fig. 6) show porous structure properties of carbons, which can be changed due to chemical activation and exfoliation. The dried nettle stem shows non-porous and macroporous property with low specific surface area. NSCNs after activation and exfoliation process can be classified as micropore materials with type I isotherm. NSCNs after exfoliating by H_2SO_4 and H_3PO_4 can be classified as wider micropore materials with type I (a) isotherm. However, NSCNs after exfoliating by HNO_3 have a quite different pore structure, becoming a type I (b) isotherm, showing wider micropores with a contribution of narrow mesopores, respectively. The qualitative property of carbon nanosheets was confirmed by SEM images and BET. The two investigations assure that carbon nanosheets were formed with a higher specific surface area (which can describe the separation ability of the carbon layer from this process) and small pore diameter.

The adsorption capacity of activated carbons is related to the surface area, pore volume, and pore size distribution. Generally, the adsorption capacity increases as the surface area of activated carbon is increased.

4
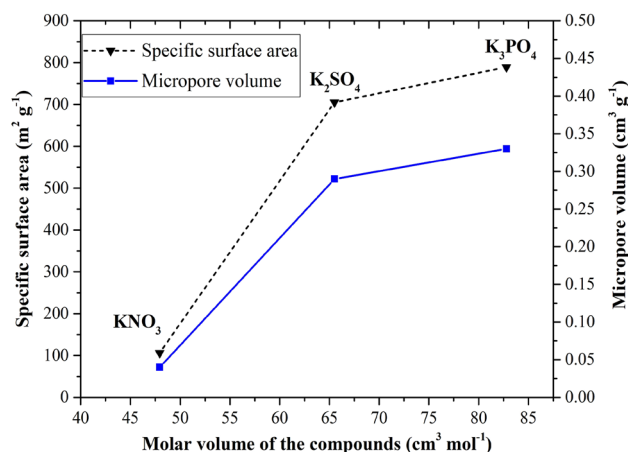
Figure 5. Relationship between molar volume of the compounds versus specific surface area and micropore volume of NSCNs after activation and exfoliation.
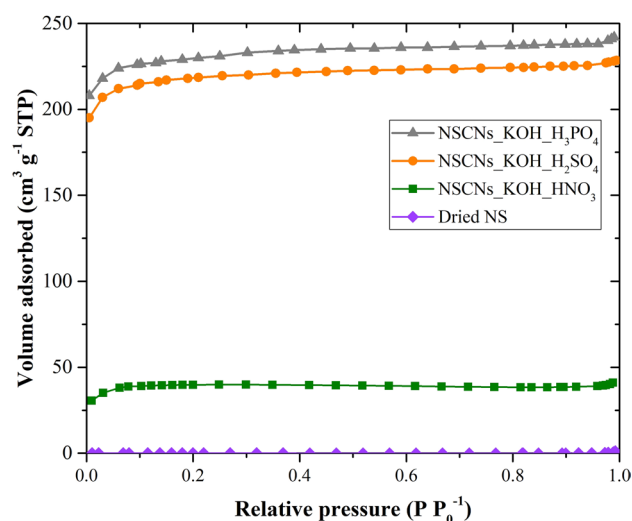

Figure 6. Nitrogen adsorption isotherms of dried NS, NSCNs exfoliated by HNO_3, H_2SO_4 or H_3PO_4.

The micropore volume of NSCNs after exfoliating by sulfuric acid and phosphoric acid is clearly higher than that of dried nettle stems. The activation and exfoliation process increased the micropore volume of the sample in the same way as the specific surface area was increased. Phosphoric acid affected the surface of NSCNs more than sulfuric acid or nitric acid due to the fact that a polyprotic acid is capable of donating more than one proton. Phosphoric acid is a triprotic acid[49] having three dissociable protons, and all three protons can be successively lost to yield $H_2PO_4^-$ followed by HPO_4^{2-} and finally PO_4^{3-}. A triprotic acid reacts with the materials more intensely than a diprotic (sulfuric acid) or monoprotic (nitric acid). The reactions result in a higher micropore volume (a more porous carbon surface), higher specific surface area and higher specific volume.

During exfoliation, cations remained in carbonaceous materials after activation reacted with the acids. The pore size distribution (Fig. 7) of NSCNs exfoliated by H_2SO_4 or H_3PO_4 is relatively uniformed, consisted of wider micropores and mesopores distributed in 2–10 nm while NSCNs exfoliated by HNO_3 mainly consisted of mesopores and small volume of micropores, and nonporous or macropores for dried nettle stem. The results were in accordance with those of the adsorption isotherms.

The BET measurements confirmed the formation of carbon nanosheets with a high specific surface area (which can describe the separation ability of carbon layer) and small pore diameter and high micropore volume. The highest specific surface area and micropore volume of NSCNs were obtained after activating with KOH and exfoliating by phosphoric acid.

Electrochemical properties. Figures 8 and 9 present the specific capacitance, energy density and power density characteristic of the electrode. The specific capacitance of NSCNs exfoliated by H_3PO_4, H_2SO_4, HNO_3 and that of char NS at a current density of 0.05 A g^{-1} was found to be 27.3, 9.34, 1.71 and 0.15 F g^{-1}, respectively. The largest specific capacitance was exhibited by the NSCNs exfoliated with H_3PO_4. The nitrogen adsorp-
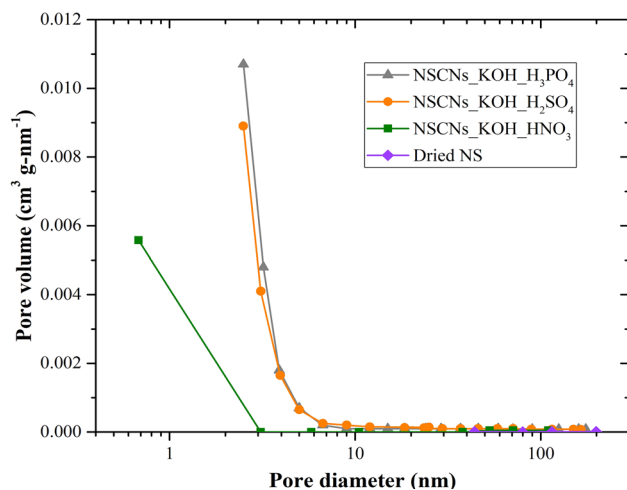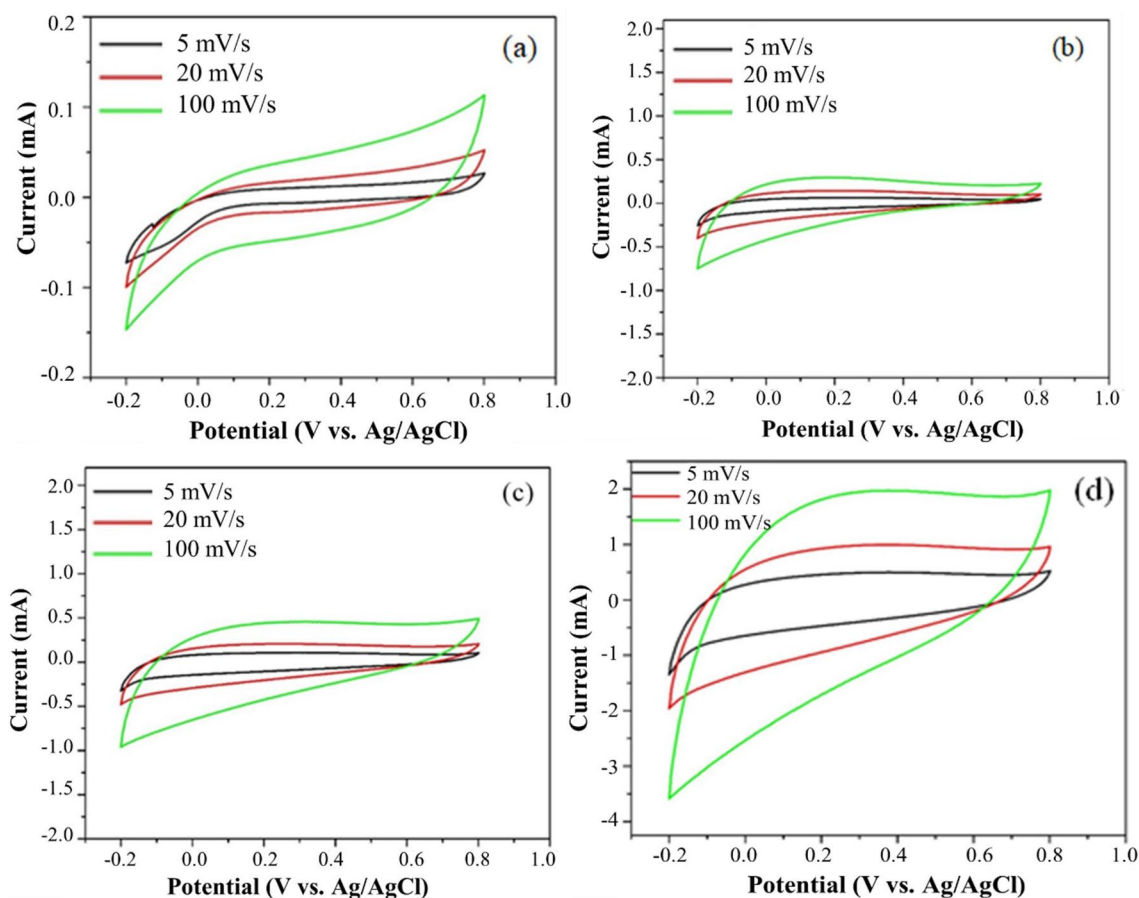
Figure 7. Pore size distribution (BJH adsorption dV/dD) of dried NS, NSCNs exfoliated by HNO_3, H_2SO_4 or H_3PO_4.
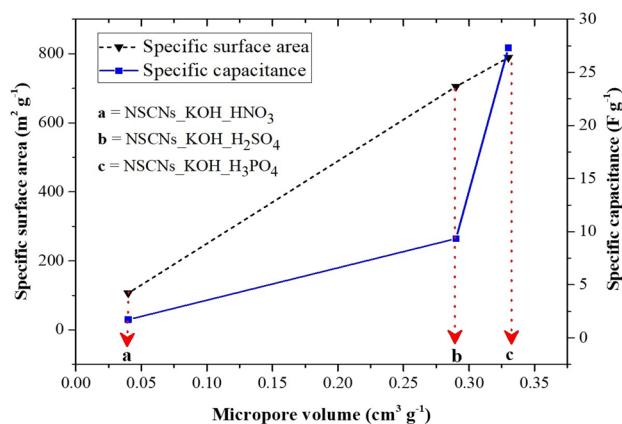
Figure 8. Specific surface area and specific capacitance of samples as a function of micropore volume.
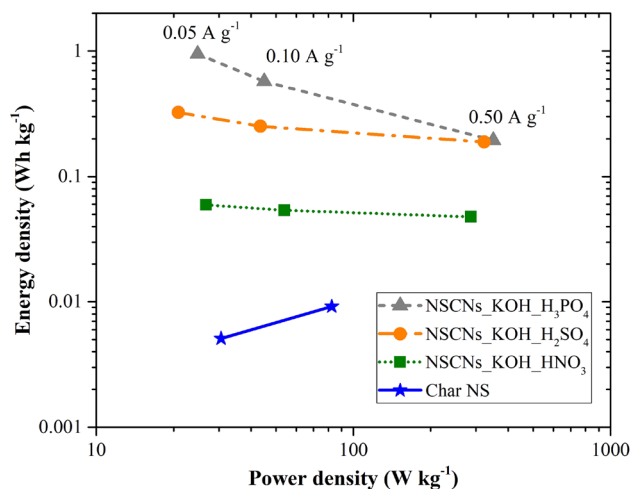
Figure 9. Energy density as a function of the power density of samples.

Figure 10. Cyclic voltammetry (CV) of nettle stem carbon nanosheets, (**a**) char NS, (**b**) exfoliated by HNO_3, (**c**) exfoliated by H_2SO_4 and (**d**) exfoliated by H_3PO_4.
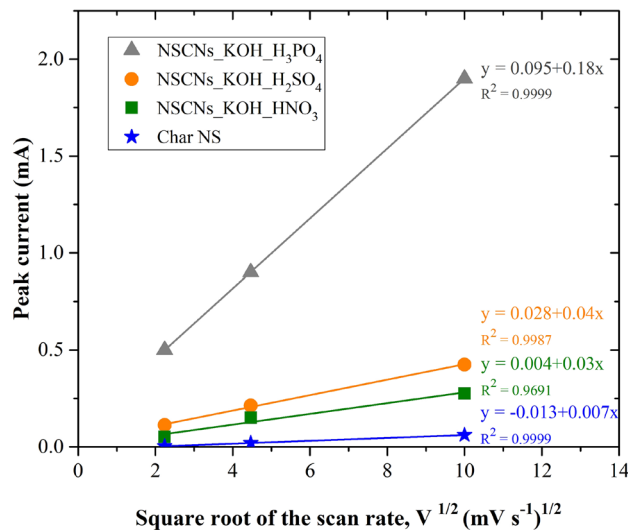
tion isotherm of NSCNs (Fig. 6) showed mostly a micropore structure according to the IUPAC classification. Micropores contain bottlenecks that can decrease ion mobility drastically, thus reducing the power capability of the electrode[50]. Porosity and surface area are directly related to capacitance, as the charge stored on the electrode surface depends on the contact established between electrode and electrolyte[51].

The specific surface area and specific capacitance of the activated and exfoliated NSCNs increase with micropore volume. The highest specific capacitance (27.3F g^{-1}) was found in NSCNs activated with KOH and exfoliated by H_3PO_4 (Fig. 8). Figure 9 shows Ragone plots demonstrating the power density and energy density of the supercapacitor electrodes. The NSCNs exfoliated by H_3PO_4 could deliver the highest energy density of 0.95 Wh kg^{-1} at a power density of 25 W kg^{-1} (at a current density of 0.05 A g^{-1}) and the highest power density of 350 W kg^{-1} at the energy density of 0.19 Wh kg^{-1} (at a current density of 0.50 A g^{-1}).

Cyclic voltammetry (CV) measurements at 5, 20 and 100 mV s^{-1} in the potential range -0.2 to 0.8 V were used to calculate the specific capacitance of carbons. CV curves show a quasi-rectangular shape at increased scan rates, indicating that the NSCNs can be used in energy storage applications[52]. The CV shape for NSCNs exfoliated with H_2SO_4 and H_3PO_4 (Fig. 10c, d) is more rectangular, revealing a better charge propagation compared to char NS (Fig. 10a), while NSCNs exfoliated with HNO_3 (Fig. 10b) showed a distorted quasi-rectangular shape. The quasi-rectangle shapes maintained even at a high scan rate of 100 mV s^{-1}, which is suitable for a typical, stable double layer capacitor that is quick and efficient in charge transfer. They also have excellent capacitive behaviour[53]. Plotting the anodic peak current (inflection point current) against square root of the scan rate shows a linear correlation (see Fig. 11), which indicates that the electrochemical process is limited by the rate of diffusion[54].

The galvanostatic charge/discharge (GCD) curves (Fig. 12) of the samples at a current density of 0.05 A g^{-1} in the voltage range of -0.2 to 0.8 V show typical triangular shapes. The GCD curves are imperfectly symmetrical; they are slightly distorted due to the pseudocapacitive behaviour[55], which is consistent with the CV graphs. The GCD curves show that NSCNs exfoliated by H_3PO_4 have the longest charge and discharge cycles, which implies the best electrochemical performance of the samples.

The electrochemical impedance spectroscopy (EIS) of NSCNs samples is presented in Fig. 13 with the Nyquist plots of each NSCNs electrode material in the frequency range between 0.1 Hz and 100 kHz. The slope of the straight line is close to 45° in the middle-high frequency and is assumed to the diffusion of the electrolyte ions in the electrode pores. The steep linear curve in the low frequency region of NSCNs is sharp, which is representative of diffusion-limited charge transfer characteristic close to ideal capacitance performance[56–59]. The equivalent series resistances (ESR) of NSCNs can be determined from the offsets on the x-axis in the high-frequency region.

$y = 0.095+0.18x$
$R^2 = 0.9999$

$y = 0.028+0.04x$
$R^2 = 0.9987$
$y = 0.004+0.03x$
$R^2 = 0.9691$
$y = -0.013+0.007x$
$R^2 = 0.9999$

Figure 11. Relationship between peak current as a function of square root of the scan rate of cyclic voltammetry measurement.
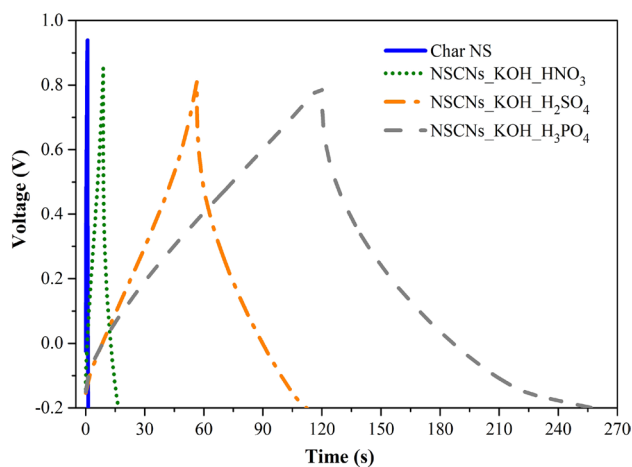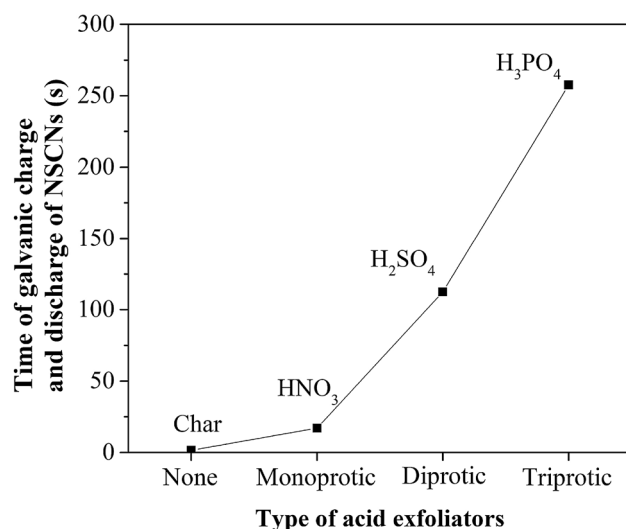

Figure 12. Galvanostatic charge/discharge of samples at a current density of 0.05 A g^{-1}.
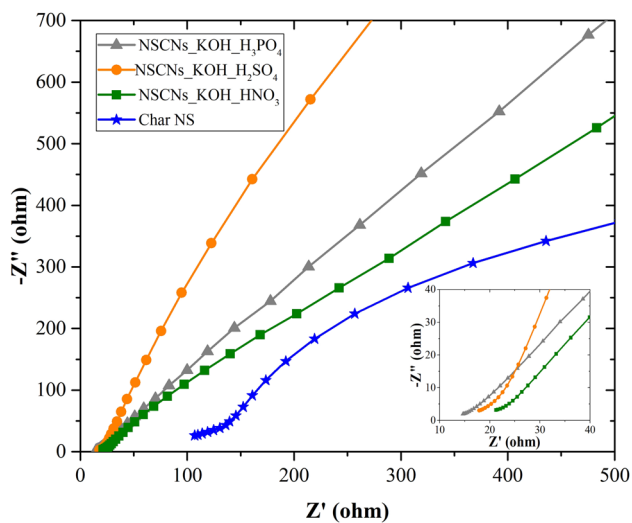
Figure 13. Nyquist plots of samples at an AC amplitude of 5 mV.

Figure 14. The time of galvanic charge and discharge of NSCNs with different types of acid exfoliators electrode.

The ESRs of NSCNs exfoliated by H_3PO_4, H_2SO_4, HNO_3 and char NS were approximately 14.6, 17.8 and 21.3 Ω, respectively, lower than that of char NS (107.0 Ω). The results confirmed the best electrochemical performance of NSCNs exfoliated by H_3PO_4. This observation is in agreement with the linear correlation between the peak current and square root of the scan rate in Fig. 11.

The increase of dissociable protons (polyprotic acid) affects the longer charge and discharge cycle time, which results has the same effect as the specific surface area. The type of acid exfoliator affected the charge and discharge cycles. Cycle time for triprotic (H_3PO_4), diprotic (H_2SO_4) and monoprotic (HNO_3) exfoliators was 260, 112 and 17 s, respectively (Fig. 14).

Conclusions

Through the preparation method proposed, carbon nanosheets were successfully synthesized using nettle stems by different acid exfoliators (HNO_3, H_2SO_4 or H_3PO_4). The morphological characteristics, chemical composition, specific surface area and micropore volume were intensively investigated. The results obtained in this work show that carbon nanosheets could be potential materials for capacitor application use as electrode material in energy storage devices. The results can be summarized as follows:

- The proposed method yields a high amount (> 80 wt.%) of carbon and clear formation of carbon nanosheet structures.
- K_3PO_4 is obtained from the reaction between the interlayered KOH residue and exfoliation acids (H_3PO_4), most likely due to its most negative ΔfG.
- Phosphoric acid exfoliates nettle stem carbon nanosheets (NSCNs) better than sulfuric acid, resulting in higher carbon content yield and higher specific surface area.
- The micropore volume of NSCNs exfoliated by phosphoric acid is higher than that of sulfuric or nitric acid; as a triprotic acid, it can react more intensively than other acids.
- Pore diameters in the exfoliated NSCNs were found to be less than 3 nm, which belongs to the micropore range (according to the IUPAC classification type I isotherm).
- NSCNs show higher specific capacitance compared to char samples (nettle stems without activation and exfoliation). The specific capacitance of NSCNs activated with KOH and exfoliated by H_3PO_4 reached 27.3 F g^{-1} at a scan rate of 5 mV s^{-1}.
- Energy density (0.06–0.95 Wh kg^{-1}) and power density (20.9–26.7 W kg^{-1}) of NSCNs (at a current density of 0.05 A g^{-1}) in this work confirmed to be supercapacitor materials.

Methods

Organic composition. The organic composition of the nettle stem, collected from Miskolc (Hungary), was investigated using chemical analysis at the commercial laboratory Mezőlabor Szolgáltató és Kereskedelmi Kft, Hungary. The acid detergent fibre content (ADF), acid detergent lignin content (ADL) and neutral detergent fibre content (NDF) were determined. The cellulose content was calculated by subtracting ADF from ADL. Similarly, hemicellulose content was calculated by subtracting NDF from ADF and lignin was calculated using ADL[35].

Synthesis of carbon nanosheets from nettle stem. The synthesis of carbon nanostructured materials from nettle stem was carried out as explained below:

- Sample preparation: The stem was chopped, washed and dried at 80 °C for 24 h followed by cleaning with HCl [0.5 M] for another 24 h. This facilitates the removal of organic compounds and residual metallic oxides[23]. It was finally washed with distilled water and dried at 80 °C for 24 h.
- Pre-Carbonization: The chopped stem was pre-carbonized (char NS) in a stainless-steel tubular furnace at 450 °C for 2 h under argon environment.
- Activation: The nettle stem was milled with a mortar for 1 h before being adding to aqueous KOH [1 M solute] with a weight ratio of 1:1 [KOH: Pre-carbonized nettle]. The mixture was stirred for an hour and dried at 80 °C for 24 h.
- Carbonization: The activated sample thus obtained was carbonized under Ar atmosphere in a tubular furnace for about 2 h. The temperature for the process was maintained at 800 °C.
- Exfoliation: The process of exfoliation was carried out by three different acids; hence, three different samples were obtained. 10 vol% each of sulfuric acid[28], phosphoric acid or nitric acid were used as exfoliators. The samples were stirred for 1 h and washed with distilled water several times until a neutral pH was obtained. The samples were then dried at 80 °C for 24 h before subjecting them to characterization tests.

Characterization. The exfoliated samples were coated with gold and investigated by scanning electron microscopy (SEM, Zeiss EVO-MA 10). The nanosheet structure was investigated by transmission electron microscopy (TEM, FEI TECNAI G2 20 X-TWIN). The chemical composition was analysed by energy-dispersive X-Ray spectrometry (EDS, EDAX Genesis). The specific surface area of the CNs was examined by Brunauer–Emmett–Teller method (BET, Micrometrics TriStar 3000) and for crystal structure X-ray Diffraction was used (XRD, Bruker D8 Advance diffractometer using Cu Kα radiation 40KV, 40 mA, in parallel beam geometry obtained with Gobel mirror, equipped with Vantec-1 position sensitive detector (1° window opening)). Patterns were recorded at 0.007° speed 2θ/29 s and within 2°–100° angular range of 2θ.

Characterization of electrochemical properties. For characterizing electrochemical properties, synthesized nettle sample, carbon black and PTFE poly-tetrafluoroethylene were weighed in a mass ratio of 90:5:5 and mixed in mortar. The electrode material was characterized by a three-electrode system of NSCNs, Pt and Ag/AgCl where the latter two are used as the counter electrode and reference electrode respectively. 1 M sodium sulphate (Na_2SO_4) aqueous solution was used as electrolyte. The electrochemical properties of the electrode material and cell were characterized by cyclic voltammetry (CV), galvanostatic charge–discharge (GCD), and electrochemical impedance spectroscopy (EIS). The specific capacitance of a symmetric supercapacitor (Cs) is calculated by the following Eq. (1)[60].

$$C_s = \frac{I \times \Delta t}{\Delta V \times m} \tag{1}$$

where $Cs, I, \Delta t, \Delta V$ and m are the specific capacitance (F g^{-1}), discharge current (A), discharge time (s), voltage change after a full charge or discharge (V) and mass of active material on electrode (g), respectively. Energy density (E, Wh kg^{-1}) (2) and power density (P, W kg^{-1}) (3) of the electrode were calculated based on the following equations:

$$E = \frac{C_s \times \Delta V^2 \times 1000}{2 \times 3600} \tag{2}$$

$$P = \frac{E}{\Delta t} \times 3600 \tag{3}$$

References

1. Fan, H. & Shen, W. Carbon nanosheets: Synthesis and application. *Chemsuschem* **8**(12), 2004–2027. https://doi.org/10.1002/cssc.201500141 (2015).
2. Singh, P., Bahadur, J. & Pal, K. One-step one chemical synthesis process of graphene from rice husk for energy storage applications. *Graphene* **6**, 61–71. https://doi.org/10.4236/graphene.2017.63005 (2017).
3. Genovese, M., Jiang, J., Lian, K. & Holm, N. High capacitive performance of exfoliated biochar nano-sheets from biomass waste corn cob. *J. Mater. Chem. A* **3**(6), 2903–2913. https://doi.org/10.1039/C4TA06110A (2015).
4. Wu, Y. *et al.* P-type boron-doped monolayer graphene with tunable bandgap for enhanced photocatalytic H_2 evolution under visible-light irradiation. *ChemCatChem* **11**(20), 5145–5153. https://doi.org/10.1002/cctc.201901258 (2019).
5. Zhu, Y. *et al.* A cocoon silk chemistry strategy to ultrathin N-doped carbon nanosheet with metal single-site catalysts. *Nat. Commun.* **9**(1), 1–9. https://doi.org/10.1038/s41467-018-06296-w (2018).
6. Zhu, Y. *et al.* A general synthetic strategy to monolayer graphene. *Nano Res.* **11**(6), 3088–3095. https://doi.org/10.1007/s12274-017-1703-3 (2018).
7. Hou, J., Cao, C., Idrees, F. & Ma, X. Hierarchical porous nitrogen-doped carbon nanosheets derived from silk for ultrahigh-capacity battery anodes and supercapacitors. *ACS Nano* **9**(3), 2556–2564. https://doi.org/10.1021/nn506394r (2015).
8. Nathan, M. I., Smith, J. E. Jr. & Tu, K. N. Raman spectra of glassy carbon. *J. Appl. Phys.* **45**(5), 2370–2370. https://doi.org/10.1063/1.1663599 (1974).
9. Wang, X. *et al.* Graphitization of glassy carbon prepared under high temperatures and high pressures. *Carbon* **41**(1), 188–191. https://doi.org/10.1016/S0008-6223(02)00319-6 (2003).

10. Kovtyukhova, N. I., Perea-López, N., Terrones, M. & Mallouk, T. E. Atomically thin layers of graphene and hexagonal boron nitride made by solvent exfoliation of their phosphoric acid intercalation compounds. *ACS Nano* **11**(7), 6746–6754. https://doi.org/10.1021/acsnano.7b01311 (2017).

11. Hong, X. & Chung, D. Exfoliated graphite with relative dielectric constant reaching 360, obtained by exfoliation of acid-intercalated graphite flakes without subsequent removal of the residual acidity. *Carbon* **91**, 1–10. https://doi.org/10.1016/j.carbon.2015.04.042 (2015).

12. Wei, T., Fan, Z., Luo, G., Zheng, C. & Xie, D. A rapid and efficient method to prepare exfoliated graphite by microwave irradiation. *Carbon* **47**(1), 337–339. https://doi.org/10.1016/j.carbon.2008.10.013 (2009).

13. Yan, Y., Kuila, T., Kim, N. & Lee, J. Effects of acid vapour mediated oxidization on the electrochemical performance of thermally exfoliated graphene. *Carbon* **74**, 195–206. https://doi.org/10.1016/j.carbon.2014.03.023 (2014).

14. Mehare, M. D., Deshmukh, A. D. & Dhoble, S. J. Preparation of porous agro-waste-derived carbon from onion peel for supercapacitor application. *J. Mater. Sci.* **55**(10), 4213–4224. https://doi.org/10.1007/s10853-019-04236-7 (2020).

15. Sun, Y. *et al.* Biomass-derived porous carbon electrodes for high-performance supercapacitors. *J. Mater. Sci.* **55**(12), 5166–5176. https://doi.org/10.1007/s10853-019-04343-5 (2020).

16. Esparza, Y., Ullah, A. & Wu, J. Preparation and characterization of graphite oxide nano-reinforced biocomposites from chicken feather keratin. *J. Chem. Technol. Biotechnol.* **92**(8), 2023–2031. https://doi.org/10.1002/jctb.5196 (2017).

17. Yahya, M. A., Al-Qodah, Z. & Ngah, C. Z. Agricultural bio-waste materials as potential sustainable precursors used for activated carbon production: A review. *Renew. Sust. Energ. Rev.* **46**, 218–235. https://doi.org/10.1016/j.rser.2015.02.051 (2015).

18. Wang, Z. *et al.* Nanocarbons from rice husk by microwave plasma irradiation: From graphene and carbon nanotubes to graphenated carbon nanotube hybrids. *Carbon* **94**, 479–484. https://doi.org/10.1016/j.carbon.2015.07.037 (2015).

19. Souza, L. K. D. *et al.* Utilization of acai stone biomass for the sustainable production of nanoporous carbon for CO_2 capture. *Sustain. Mater. Technol.* https://doi.org/10.1016/j.susmat.2020.e00168 (2020).

20. Romanos, J. *et al.* Nanospace engineering of KOH activated carbon. *Nanotechnology* **23**(1), 015401. https://doi.org/10.1088/0957-4484/23/1/015401 (2011).

21. Nagaraju, G., Cha, S. M. & Yu, J. S. Ultrathin nickel hydroxide nano-sheet arrays grafted biomass-derived honeycomb-like porous carbon with improved electrochemical performance as a supercapacitive material. *Sci. Rep.* **7**, 45201. https://doi.org/10.1038/srep45201 (2017).

22. Li, F. *et al.* Hierarchically porous carbon derived from banana peel for lithium sulphur battery with high areal and gravimetric sulphur loading. *J. Power Sources* **362**, 160–167. https://doi.org/10.1016/j.jpowsour.2017.07.038 (2017).

23. Wu, K. *et al.* Large and porous carbon sheets derived from water hyacinth for high-performance supercapacitors. *RSC Adv.* **6**(36), 29996–30003. https://doi.org/10.1039/C5RA25098F (2016).

24. Liu, X. *et al.* High yield conversion of biowaste coffee grounds into hierarchical porous carbon for superior capacitive energy storage. *Sci. Rep.* **10**, 3518. https://doi.org/10.1038/s41598-020-60625-y (2020).

25. Sodtipinta, J., Amornsakchai, T. & Pakawatpanurut, P. Nanoporous carbon derived from agro-waste pineapple leaves for supercapacitor electrode. *Adv. Nat. Sci. Nanosci. Nanotechnol.* **8**(3), 035017. https://doi.org/10.1088/2043-6254/aa7233 (2017).

26. Gu, X. *et al.* Microporous bamboo biochar for lithium-sulfur batteries. *Nano Res.* **8**(1), 129–139. https://doi.org/10.1007/s12274-014-0601-1 (2015).

27. Yargic, A. S. & Ozbay, N. Effect of chemical activation on the cellular structure of biopitch-derived green carbon foam. *Diam. Relat. Mater.* **96**, 58–66. https://doi.org/10.1016/j.diamond.2019.04.032 (2019).

28. Purkait, T., Singh, G., Singh, M., Kumar, D. & Dey, R. S. Large area few-layer graphene with scalable preparation from waste biomass for high-performance supercapacitor. *Sci. Rep.* **7**(1), 15239. https://doi.org/10.1038/s41598-017-15463-w (2017).

29. Yallappa, S. *et al.* Natural biowaste of groundnut shell derived nano carbons: Synthesis, characterization and its in vitro antibacterial activity. *Nano-Struct. Nano-Obj.* **12**, 84–90. https://doi.org/10.1016/j.nanoso.2017.09.009 (2017).

30. Nuilek, K., Simon, A. & Baumli, P. Influence of KOH on the carbon nanostructure of peanut shell. *Resolut. Discov.* **3**(2), 29–32. https://doi.org/10.1556/2051.2018.00060 (2018).

31. Khan, J. H. *et al.* Jute-derived microporous/mesoporous carbon with ultra-high surface area using a chemical activation process. *Microporous Mesoporous Mater.* **274**, 251–256. https://doi.org/10.1016/j.micromeso.2018.07.050 (2019).

32. Li, S., Han, K., Li, J., Li, M. & Lu, C. Preparation and characterization of super activated carbon produced from gulfweed by KOH activation. *Microporous Mesoporous Mater.* **243**, 291–300. https://doi.org/10.1016/j.micromeso.2017.02.052 (2017).

33. Han, J. *et al.* One-step nitrogen, boron codoping of porous carbons derived from pomelo peels for supercapacitor electrode materials. *Diam. Relat. Mater.* **96**, 176–181. https://doi.org/10.1016/j.diamond.2019.05.014 (2019).

34. Di Virgilio, N. *et al.* The potential of stinging nettle (*Urtica dioica* L.) as a crop with multiple uses. *Ind. Crops. Prod.* **68**, 42–49. https://doi.org/10.1016/j.indcrop.2014.08.012 (2015).

35. Bacci, L., Baronti, S., Predier, S. & Di Virgilio, N. Fibre yield and quality of fibre nettle (*Urtica dioica* L.) cultivated in Italy. *Ind. Crops. Prod.* **29**(2–3), 480–484. https://doi.org/10.1016/j.indcrop.2008.09.005 (2009).

36. Cagnon, B., Py, X., Guillot, A., Stoeckli, F. & Chambat, G. Contributions of hemicellulose, cellulose and lignin to the mass and the porous properties of chars and steam activated carbons from various lignocellulosic precursors. *Bioresour. Technol.* **100**, 292–298. https://doi.org/10.1016/J.BIORTECH.2008.06.009 (2009).

37. Thomas, P., Lai, C. W. & Bin Johan, M. R. Recent developments in biomass-derived carbon as a potential sustainable material for super-capacitor-based energy storage and environmental applications. *J. Anal. Appl. Pyrolysis.* **140**, 54–85. https://doi.org/10.1016/j.jaap.2019.03.021 (2019).

38. Fan, W. *et al.* Dual-doped hierarchical porous carbon derived from biomass for advanced supercapacitors and lithium ion batteries. *RSC Adv.* **9**(56), 32382–32394. https://doi.org/10.1039/C9RA06914C (2019).

39. Stoller, M. D., Park, S., Zhu, Y., An, J. & Rouf, R. S. Graphene-based ultracapacitor. *Nano Lett.* **8**(10), 3498–3502. https://doi.org/10.1021/nl802558y (2008).

40. Wu, H. P. *et al.* Graphene as the electrode material in supercapacitors. *(In 2010 8th International Vacuum Electron Sources Conference and Nanocarbon) IEEE.* 465–466, https://doi.org/10.1109/IVESC.2010.5644267 (2020).

41. Ghosh, S. *et al.* Natural biomass derived hard carbon and activated carbons as electrochemical supercapacitor electrodes. *Sci. Rep.* **9**(1), 16315. https://doi.org/10.1038/s41598-019-52006-x (2019).

42. Emmenegger, C. *et al.* Investigation of electrochemical double-layer (ECDL) capacitors electrodes based on carbon nanotubes and activated carbon materials. *J. Power Sources* **124**(1), 321–329. https://doi.org/10.1016/S0378-7753(03)00590-1 (2003).

43. Suhas, *et al.* Cellulose: A review as natural, modified and activated carbon adsorbent. *Bioresour. Technol.* **216**, 1066–1076. https://doi.org/10.1016/j.biortech.2016.05.106 (2016).

44. Park, M. H., Kim, N. R., Yun, Y. S., Cho, S. Y. & Jin, H. J. Waste coffee grounds-derived nanoporous carbon nanosheets for supercapacitors. *Carbon Lett.* **19**, 66–71. https://doi.org/10.5714/CL.2016.19.066 (2016).

45. Jacobsen, A. J., Mahoney, S., Carter, W. B. & Nutt, S. Vitreous carbon micro-lattice structures. *Carbon* **49**(3), 1025–1032. https://doi.org/10.1016/j.carbon.2010.10.059 (2011).

46. Cowlard, F. C. & Lewis, J. C. Vitreous carbon—A new form of carbon. *J. Mater. Sci.* **2**(6), 507–512. https://doi.org/10.1007/BF00752216 (1967).

47. Outokumpu HSC Chemistry for Windows, version 6.0; Outokumpu Research Oy: Pori, Finland (2006).

48. Thommes, M. *et al.* Physisorption of gases, with special reference to the evaluation of surface area and pore size distribution (IUPAC Technical Report). *Pure Appl. Chem.* **87**(9–10), 1051–1069. https://doi.org/10.1515/pac-2014-1117 (2015).
49. Cegla, R. N. R. *et al.* Comparative study of conversion of coral with ammonium dihydrogen phosphate and orthophosphoric acid to produce calcium phosphate. *J. Aust. Ceram. Soc.* **50**(2), 154–161 (2014).
50. González, A., Goikolea, E., Barrena, J. A. & Mysyk, R. Review on supercapacitors: Technologies and materials. *Renew. Sust. Energ. Rev.* **58**, 1189–1206. https://doi.org/10.1016/j.rser.2015.12.249 (2016).
51. Mishra, N. *et al.* MWCNTs synthesized from waste polypropylene plastics and its application in super-capacitors. *AIP Conf. Proc.* **1538**(1), 228–236. https://doi.org/10.1063/1.4810063 (2013).
52. Divyashree, A. & Hegde, G. Activated carbon nanospheres derived from bio-waste materials for supercapacitor applications—A review. *Rsc Adv.* **5**(107), 88339–88352. https://doi.org/10.1039/C5RA19392C (2015).
53. Wang, X., Zhou, X., Chen, W., Chen, M. & Liu, C. Enhancement of the electrochemical properties of commercial coconut shell-based activated carbon by H_2O dielectric barrier discharge plasma. *R. Soc. Open Sci.* **6**(2), 180872. https://doi.org/10.1098/rsos.180872 (2019).
54. Ensafi, A. A., Rezaei, B., Mirahmadi-Zare, Z. & Karimi-Maleh, H. Highly selective and sensitive voltammetric sensor for captopril determination based on modified multiwall carbon nanotubes paste electrode. *J. Braz. Chem. Soc.* **22**(7), 1315–1322. https://doi.org/10.1590/S0103-50532011000700017 (2011).
55. Azman, N. H. N. & Mamat@ Mat Nazir, M. S., Ngee, L. H. & Sulaiman, Y. ,. Graphene-based ternary composites for supercapacitors. *Int. J. Energ. Res.* **42**(6), 2104–2116. https://doi.org/10.1002/er.4001 (2018).
56. Chen, X. *et al.* A novel hierarchical porous nitrogen-doped carbon derived from bamboo shoot for high performance supercapacitor. *Sci. Rep.* **7**(1), 1–11. https://doi.org/10.1038/s41598-017-06730-x (2017).
57. Li, Y. *et al.* Fabrication of manganese dioxide nanoplates anchoring on biomass-derived cross-linked carbon nanosheets for high-performance asymmetric supercapacitors. *J. Power Sources* **300**, 309–317. https://doi.org/10.1016/j.jpowsour.2015.09.077 (2015).
58. Chen, L., Ji, T., Brisbin, L. & Zhu, J. H. Hierarchical porous and high surface area tubular carbon as dye adsorbent and capacitor electrode. *ACS Appl. Mater. Interfaces* **7**, 12230–12237. https://doi.org/10.1021/acsami.5b02697 (2015).
59. Sivachidambaram, M. *et al.* Preparation and characterization of activated carbon derived from the *Borassus flabellifer* flower as an electrode material for supercapacitor applications. *New J. Chem.* **41**(10), 3939–3949. https://doi.org/10.1039/c6nj03867k (2017).
60. Sattayarut, V. *et al.* Preparation and electrochemical performance of nitrogen-enriched activated carbon derived from silkworm pupae waste. *RSC Adv.* **9**(18), 9878–9886. https://doi.org/10.1039/C9RA01090D (2019).

Acknowledgements

Author contributions

K.N., A.S. and P.B. planned and designed the experiments, wrote the main text of the manuscript and made final evaluations of the results. W.W. and V.S. did the electrochemical tests and evaluation of the results. D.K.-H. analysed the samples in the SEM investigations. T.F. did the BET tests. F.K. carried out the XRD measurements and evaluations. All authors reviewed the manuscript.

Competing interests

The authors declare no competing interests.

Additional information

Correspondence and requests for materials should be addressed to K.N. or P.B.

Reprints and permissions information is available at www.nature.com/reprints.

Publisher's note Springer Nature remains neutral with regard to jurisdictional claims in published maps and institutional affiliations.